Coupled Systems Mechanics, *Vol. 14, No. 3 (2025) 289-312*
https://doi.org/10.12989/csm.2025.14.3.289

Analysis of equilibrium phase and the geometric design of metal foam plates

Nabil Himeur[1,2a], Messaoud Baazouzi[3,4a], Khawla Boudiaf[3,4a], Mohamed Tabet[3,4a], Dalila Kamli[5,6b], Abderrahmane Menasria[3,7a] and Abdelhakim Bouhadra*[3,7]

[1]*Mechanical Engineering Department, Faculty of Science & Technology, University Abbes Laghrour, Khenchela 40000, Algeria*
[2]*Laboratory of Engineering and Sciences of Advanced Materials (ISMA), Abbes Laghrour University Khenchela, 40004, Algeria*
[3]*Civil Engineering Department, Faculty of Sciences & Technology, University Abbes Laghrour, Khenchela 40000, Algeria*
[4]*Civil Engineering Research Laboratory LRGC, Biskra University, 07000 Biskra, Algeria*
[5]*Laboratory of Electrochemistry, Molecular Engineering and Redox Catalysis (LEIMCR), Department of Basic Technology Education, Faculty of Technology, Ferhat Abbas University, Sétif-1, Algeria*
[6]*Department of Material Sciences, Faculty of Sciences & Technology, University of Khenchela, Algeria*
[7]*Material and Hydrology Laboratory, Civil Engineering Department, Faculty of Technology, Djillali Liabes University, Sidi Bel Abbes 22000, Algeria*

(Received May 29, 2025, Revised July 13, 2025, Accepted July 14, 2025)

Abstract. This study employs an advanced four-variable plate theory to examine the mechanical bending response of simply supported rectangular metal foam plates. With the rise of composite materials in the aerospace, automotive, and transportation sectors, there is a need for analytical techniques to model their performance in various environments. Functionally graded porous plates (FGPs) are composites with gradual variations in porosity. Nevertheless, few studies have systematically investigated the effects of geometric parameters and mechanical loadings on the mechanical properties of metal foam plates using plate theory. The aim of this study is to shed the light on the elastic bending behavior of imperfect plates under sinusoidal loading by applying a refined plate theory that incorporates both bending and shear components of transverse displacement into the kinematic framework. This formulation simplifies structural analysis by reducing the number of governing equations. Specifically, we analyze a simply supported imperfect metal-foam plate with two distinct porosity levels subjected to a sinusoidally distributed load. The results reveal intricate dependencies between plate geometry, thickness, and deflection behavior, including critical transitions at specific thickness ratios. The refined plate theory closely matches higher-order shear deformation theories, thereby justifying its accuracy and reliability. The findings advance the understanding of metal foam plate mechanics and enhance the design of structures particularly in aerospace and automotive engineering where accurate prediction of plate behavior is essential.

Keywords: geometric parameters; mechanical bending; metal foam plates; refined plate theory; semi-analytical approach; sinusoidal loading

*Corresponding author, Professor, E-mail: abdelhakim.bouhadra@univ-khenchela.dz

http://www.techno-press.org/?journal=csm&subpage=8 ISSN: 2234-2184 (Print), 2234-2192 (Online)

1. Introduction

Key innovations are often predicated on the need for lighter, stronger, and more durable structures, particularly in energy-hungry sectors such as aerospace and transportation. This challenge effectively found its way into Functionally Graded Materials (FGMs), which tend to combine a gradual change in material properties throughout their thickness (Koizumi 1997). Traditional laminated composite designs usually incorporate undesirable stress discontinuities at the interfaces between two successive composite layers, resulting in local approachability and stress concentrations. In contrast, in cases of FGMs, a smooth transition of the material properties can be achieved, thus eliminating the stress concentrations in engineering applications, particularly where high thermal gradients or complex stress distributions are present (Loh *et al*. 2018, Zhang *et al.* 2022). This structural characteristic distinctly sets FGMs apart and renders them ideally suited for applications that necessitate intricate mapping of material properties under extreme environmental conditions and complex loading profiles. With the latest developments in additive manufacturing, the use of FGMs has changed drastically, as more control can be achieved over the material composition and distribution within 3D structures (Garg *et al*. 2022, Wei *et al*. 2023). AM has empowered engineering by allowing material-controlled deposition and the production of smooth, homogeneous structures with intricately varying densities and orientations. Such innovations broaden the scope of FGMs, enabling their integration into various facets of engineering, such as the construction of lighter and more fuel-efficient vehicles and airplanes.

In recent years, the inclusion of metal foams in FGM structures, especially in the sandwich configuration, has garnered significant attention (Adhikari *et al*. 2020, Tamrabet *et al.* 2023). Metal foams are advantageous as core materials in sandwich structures because of their lightweight and energy absorption capabilities (Singh and Harsha 2021, Sinha and Kumar 2021). The combination of functionally graded materials, whose microstructure is finely designed, and metal foams, which have excellent specific strength and impact resistance, has opened new avenues for development in aerospace, automotive, and civil engineering (Himeur *et al*. 2022, Hu *et al.* 2023). The possibility of thinner but stronger structures with improved performance under multiple loading conditions has motivated the investigation of FGM sandwich structures with metal foam cores. This has increased research efforts to understand their distinct and intricate mechanical behaviors and design them for specific engineering problems. Finally, this study is expected to enhance the safety and efficiency of transportation systems and infrastructure in a more globally sustainable manner.

The research and development of FGM plates, especially those with metal foam cores, is significant because of their applications in different industries (Menasria *et al*. 2024, Messaoudi *et al.* 2023, Zhou *et al*. 2022). Owing to the structure of the material gradient and porous core, the complexity of these components makes it essential to develop advanced analytical models to adequately describe their mechanical behavior. Various plate theories have been established and enhanced to model the intricate mechanical response of these structures under diverse loading conditions and boundary constraints (Chen *et al*. 2017, Slimani *et al*. 2024). Recently, many studies have predominantly focused on modeling and analyzing functionally graded (FG) or orthotropic layered media under various mechanical and thermal loads, often employing analytical, numerical (FEM), and increasingly hybrid artificial intelligence approaches. Yaylacı *et al.* (2025) evaluated frictionless contact between a circular rigid punch and a two-layer FG system on a Pasternak foundation, combining analytical, FEM, and multilayer perceptron (MLP) methods. Aktarer *et al.* (2025) examined the microstructure and mechanical changes in DP800 steel

processed using multiphases friction stir methods. Yaylaci *et al.* (2024) examined a two-dimensional crack problem in a half-infinite functionally graded layer pressed between two rigid blocks using the finite element method (FEM) via ANSYS and an artificial neural network (ANN) with a multilayer perceptron (MLP). Yaylacı *et al.* (2024) A companion study compared analytical and numeric the Conta half-plane configuration. (Fuyad *et al.* 2024) examined a cantilever beam using a nonlinear dynamic elastic-plastic framework to explore ratcheting under varying primary/secondary bending loads. Sekban *et al.* (2025) investigated the formability of friction stir–welded high-strength shipbuilding steel by combining experiments, FEM, and neural networks. In advanced materials research, a study on piezo-magneto-thermoelastic FG nanobeams submerged in fluid explored vibrational behavior using higher-order strain gradient theory have been realized by Rajendran *et al.* (2024). Öner *et al.* (2024) performed a ratcheting analysis on beams subjected to combined bending loads, revealing frequency dependence in strain accumulation. Selvamani *et al.* (2024) used a multiple-scale perturbation method to study nonlinear wave propagation in doubly curved sandwich composite piezoelectric shells with a flexible core subjected to hygrothermal conditions. Sekban *et al.* (2024) studied the FSP of AH32 shipbuilding steel- using mechanical tests, finite element simulations, and neural network models. All three assessment methods showed a significant strength improvement, minimal loss in formability, and strong agreement. Yaylacı *et al.* (2024) filled a gap by examining both continuous and discontinuous contact problems involving an FG layer resting on a rigid foundation and subjected to a rigid punch. Using both analytical and finite element methods (FEM), the study evaluated the contact length, stress, separation distance, and points of detachment. Selvamani *et al.* (2024) focused on modeling and analyzing the nonlinear vibration patterns and parametric excitation of embedded Euler–Bernoulli nanobeams (EBNB) subjected to thermo-magneto-mechanical loads. Sekban *et al.* (2024) investigated friction stir welding (FSW) on ship-grade steel and performed hardness, tensile, and bending tests to evaluate its mechanical performance. The bending test results, which are critical for assessing weld formability, were subsequently used to train both finite element analysis (FEA) and multilayer perceptron (MLP) models.

Tounsi *et al.* (2025) developed a quasi-3D plate theory incorporating size-dependent effects via a modified couple stress to analyze the static behavior and free vibration of porous functionally graded (FG) microplates. Lakhdar *et al.* (2024) presented a novel integral Timoshenko theory to investigate free vibration in imperfect FG beams. Gawah *et al.* (2025) explored wave propagation in graphene platelet-reinforced- FG porous plates on viscoelastic foundations using an integral higher-order shear deformation theory (HSDT). Kaddari *et al.* (2025) examined the effect of porosity distribution on buckling in FG sandwich plates via a quasi-3D refined plate theory. Tounsi *et al.* (2024) studied the free vibration of FG sandwich plates under different boundary conditions and hygro-thermal environments resting on viscoelastic foundations. Earlier, Tounsi *et al.* (2023) investigated the free vibration of temperature-dependent FG plates on viscoelastic foundations. Youzera *et al.* (2025) analyzed free vibration in cylindrical sandwich shells with FG carbon nanotube-reinforced composite face sheets using the differential quadrature method. Tounsi *et al.* (2023) introduced an integral quasi-3D model for hygro-thermal wave propagation in imperfect FG sandwich plates. (Addou *et al.* 2023) assessed how porosity distribution influences the static behavior of FG plates using a simplified quasi-3D HSDT. Mudhaffar *et al.* (2023) investigated the bending behavior of FG plates on viscoelastic foundations under hygro-thermo-mechanical loads. Kadiri *et al.* (2024) addressed wave propagation in FG polymer composite nanoplates embedded in a variable elastic medium. Driz *et al.* (2024) studied the dynamic response of imperfect FG plates, focusing on graded patterns and viscoelastic

foundations. Lakhdar *et al*. (2024) further examined free vibration and bending in porous bi-directional FG sandwich shells using third-order shear deformation theory (TSDT) and p-version finite elements. Finally, Bentrar *et al*. (2023) explored the effects of porosity distribution on the free vibration of FG sandwich plates using p-version finite element modeling. Xiong *et al*. (2022) introduced a novel analytical solution for the thermal stability of moderately thick FG plates with temperature-dependent material properties using non-Levy- boundary conditions and employing a symplectic superposition method based on Hamiltonian mechanics. Hu *et al.* (2024) provided mathematically rigorous, benchmark-quality analytical expressions for the free vibration behavior of cracked FGM plates, enabling accurate prediction without extensive numerical or experimental effort. Xiong *et al.* (2022) investigated the thermal buckling behavior of non-Levy-type functionally graded (FG) rectangular plates using a novel Symplectic Superposition Method (SSM), which was formulated within the symplectic-space Hamiltonian framework.

However, the assessment of FGM sandwich structures with metal foam cores, particularly those with skewed configurations, remains substantially unexplored, impeding the full potential of these materials in diverse engineering applications. Contemporary studies have made progress in formulating rigorous and optimized analytical models for FGM plates with metal foam cores. For instance, Chen *et al*. (2019) evaluated the bending and buckling behaviors of FG sandwich plates with closed-cell aluminum foam cores using the Chebyshev-Ritz method. (Garg *et al.* 2022, Tamrabet *et al.* 2024) analyzed the impact of different porosity distributions in metal the stability and free vibration of FGM sandwich plates vibration using a zigzag theory formulation. The influence of resilient foundations on the mechanical response of FGM structures has received substantial attention. Himeur *et al*. (2022) explored the coupled effect of variable Winkler-Pasternak foundations on the bending behavior of FGM plates subjected to various loading types. Their study demonstrated the substantial impact of foundation parameters on plate deflections and stress distributions, emphasizing the importance of incorporating foundation interactions into practical applications.

The considerable influence of porosity on the mechanical properties of FGM sandwich plates with metal foam cores has been the focus of multiple studies. Various studies have demonstrated the critical effects of porosity on the stability response and oscillation characteristics of these structures (Adhikari *et al*. 2020, Garg *et al.* 2022). These studies have shown that porosity can considerably decrease the rigidity of a structure, reducing the essential stability load and changing the oscillation frequencies (Chen *et al.* 2016, Yıldız 2024). Comprehending the complex relationship between porosity and the mechanical properties of FGM sandwich plates is necessary for enhancing their design and maintaining their structural performance under various loading conditions. Chen *et al*. (2016) used the Ritz method to examine the influence of irregular porosity distribution on the natural and induced oscillations of functionally modified beams, demonstrating that porosity distribution can significantly affect the motion characteristics of these structures.

The dynamic behavior of FGM plates with metal foam cores has also been thoroughly examined. Current research has investigated free vibration and dynamic stability under diverse conditions (Dung *et al.* 2021, Mantari *et al*. 2012). For example, Zhou *et al*. (2022) performed a nonlinear vibration analysis of gradually modified flow pipelines under standard boundary conditions. Such studies offer essential insights into the performance of these materials under dynamic loading scenarios, which is especially important for applications in aerospace, transportation, and other industries in which structures experience motion excitations. The combination of piezoelectric adaptive materials with FGMs has increased the potential for innovative engineering applications. Yıldız (2024) analyzed the heat-mechanical oscillation

behavior of adaptive nanosensor plates incorporating both dense and foam structures, examining a significant gap in understanding the heat-mechanical behavior of adaptive nanoplates with foam structures.

The development of two-variable refined plate theories has demonstrated substantial progress in their capability to provide accurate results with notably decreased computational complexity (Kar *et al*. 2015, Nguyen *et al.* 2019). These theories have been effectively applied to analyze FGM plates with metal foam cores, presenting an optimal balance between accuracy and computational efficiency (Ansari *et al*. 2015, Garg and Chalak 2019). By incorporating deformation effects and minimizing the number of variables, these advanced theories establish a computationally efficient alternative to complex 3D models, rendering them especially valuable for engineering applications in which computational resources are constrained.

Despite these developments, a crucial gap exists in the thorough analysis of FGM sandwich structures, specifically incorporating metal foam cores. While substantial progress has been achieved in examining the behavior of metal foam cores in sandwich structures, an enhanced understanding of the structural stability of imperfect FG sandwich plates, particularly regarding the thickness-stretching effects in thick plates, remains essential. Furthermore, the thermomechanical behavior of smart nanoplates with foam structures requires more extensive investigation, particularly in the context of cutting-edge sensing and monitoring applications (Berkia *et al.* 2022, Nguyen *et al*. 2018, Nguyen *et al*. 2019, Sun *et al.* 2019, Tounsi *et al*. 2017, Van Vinh 2022, Zahari *et al.* 2022).

In this study, we present a static analysis of metal-foam plates subjected to a sinusoidally distributed load using a refined plate theory that incorporates two components of transverse displacement bending and shear into the kinematic model. This approach reduces the number of governing equations and streamlines the structural analysis. Two levels of porosity were considered in the analysis. Their mechanical properties, such as Young's modulus and Poisson's ratio, are crucial in determining their behavior under various loading conditions. To achieve this research objective, a static analysis of these plates was conducted, and the equilibrium equations were derived by applying the principle of virtual work. Mathematical expressions for the deflection, normal stresses, and tangential stresses are obtained using Navier's approach to solve the system of equilibrium equations.

2. Section headings

2.1 Refined plate's theory

2.1.1 Geometric configuration

Fig. 1 shows a supported metal foam rectangular plate with length a, width b, and thickness h. The coordinate system was defined such that the x- and y-axes lie in the plane of the plate, whereas the z-axis is oriented in the thickness direction. The midplane of the rectangular metal foam plate was defined as $z=0$. The lower and upper surfaces of the plate are located at $z=-h/2$ and $z=h/2$.

This study investigates the flexural behavior of supported metal-foam rectangular plates subjected to sinusoidally distributed mechanical loads. This analysis provides insights into the response of the plate under specific loading conditions, contributing to a broader understanding of structural mechanics in plate theory.

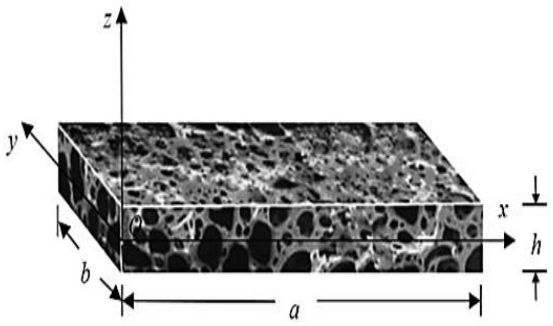

Fig. 1 Geometry of metal foam plate

2.1.2 Material distribution

$$\begin{cases} E = E_1\eta \\ G = G_1\eta \end{cases} \tag{1}$$

where the shear modulus G and Young's modulus E along the thickness are constant.

E_1 and G_1 are the Young's and shear moduli of the metal without internal pores, respectively, η is the porosity for uniform porosity distribution, such as $\eta\epsilon[0.6012, 0.9360]$ for our purpose.

2.1.3 Fundamental assumptions

The refined plate theory presented herein is based on the following assumptions:

The displacements were small relative to the plate thickness, resulting in infinitesimal strains.

The transverse displacement W comprises bending (w_b), and shear (w_s). These components are functions of the x and y coordinates.

$$W(x, y, z) = w_b(x, y) + w_s(x, y) \tag{2}$$

The transverse normal stress σ_z is negligible compared to the in-plane stresses σ_x and σ_y.

The displacements U in the x-direction and V in the y-direction are defined by the superposition of the displacements owing to the extension, bending, and shear effects

$$\begin{aligned} U &= u + u_b + u_s \\ V &= v + v_b + v_s \end{aligned} \tag{3}$$

The bending components u_b and v_b are assumed to be the same as the displacements given by the classical plate theory. Thus, the expressions for u_b and v_b can be written as

$$\begin{aligned} u_b &= -z\frac{\partial w_b}{\partial x} \\ v_b &= -z\frac{\partial w_b}{\partial y} \end{aligned} \tag{4a}$$

From the displacement state of the components us and vs, the shear strain components γ_{xz} and γ_{yz} are derived. These components vary parabolically through the plate thickness while ensuring zero shear stresses τ_{xz} and τ_{yz} at the lower and upper surfaces of the plate. Consequently, the expressions for us and vs can be expressed as

$$u_s = \left[\frac{1}{4}z - \frac{5}{3}z\left(\frac{z}{h}\right)^2\right]\frac{\partial w_s}{\partial x}$$
$$v_s = \left[\frac{1}{4}z - \frac{5}{3}z\left(\frac{z}{h}\right)^2\right]\frac{\partial w_s}{\partial y} \tag{4b}$$

2.2 Kinematic and constitutive equations

Based on the assumptions presented in the previous section, the displacement field can be derived using Eqs. (2)-(4) as follows

$$\begin{cases} U(x,y,z) = u(x,y) - z\dfrac{\partial w_b}{\partial x} + z\left[\dfrac{1}{4} - \dfrac{5}{3}\left(\dfrac{z}{h}\right)^2\right]\dfrac{\partial w_s}{\partial x} \\ V(x,y,z) = v(x,y) - z\dfrac{\partial w_b}{\partial y} + z\left[\dfrac{1}{4} - \dfrac{5}{3}\left(\dfrac{z}{h}\right)^2\right]\dfrac{\partial w_s}{\partial y} \\ W(x,y,z) = w_b(x,y) + w_s(x,y) \end{cases} \tag{5}$$

The strain field is derived from the displacements in Eq. (5) as follows

$$\varepsilon_x = \varepsilon_x^0 + zk_x^b + \left[-\frac{1}{4}z + \frac{5}{3}z\left(\frac{z}{h}\right)^2\right]k_x^s$$
$$\varepsilon_y = \varepsilon_y^0 + zk_y^b + \left[-\frac{1}{4}z + \frac{5}{3}z\left(\frac{z}{h}\right)^2\right]k_y^s$$
$$\gamma_{xy} = \gamma_{xy}^0 + zk_{xy}^b + \left[-\frac{1}{4}z + \frac{5}{3}z\left(\frac{z}{h}\right)^2\right]k_{xy}^s \tag{6}$$
$$\gamma_{yz} = \left[\frac{5}{4} - 5\left(\frac{z}{h}\right)^2\right]\gamma_{yz}^s$$
$$\gamma_{xz} = \left[\frac{5}{4} - 5\left(\frac{z}{h}\right)^2\right]\gamma_{xz}^s$$

Where

$$\varepsilon_x^0 = \frac{\partial u}{\partial x}, \qquad k_x^b = -\frac{\partial^2 w_b}{\partial x^2}, \qquad k_x^s = -\frac{\partial^2 w_s}{\partial x^2}, \tag{7a}$$

$$\gamma_{xy}^0 = \frac{\partial u}{\partial y} + \frac{\partial v}{\partial x}, \qquad k_{xy}^b = -2\frac{\partial^2 w_b}{\partial x\,\partial y}, \tag{7b}$$

$$\varepsilon_y^0 = \frac{\partial v}{\partial y}, \tag{7c}$$

$$k_{xy}^s = -2\frac{\partial^2 w_s}{\partial x\,\partial y}, \qquad \gamma_{yz}^s = \frac{\partial w_s}{\partial y}, \qquad \gamma_{xz}^s = \frac{\partial w_s}{\partial x}, \tag{7d}$$

For elastic metal foam plates, the constitutive relations can be expressed as

$$\begin{Bmatrix}\sigma_x\\ \sigma_y\\ \tau_{xy}\end{Bmatrix}=\begin{bmatrix}Q_{11} & Q_{12} & 0\\ Q_{12} & Q_{22} & 0\\ 0 & 0 & Q_{66}\end{bmatrix}\begin{Bmatrix}\varepsilon_x\\ \varepsilon_y\\ \gamma_{xy}\end{Bmatrix} \tag{8a}$$

$$\begin{Bmatrix}\tau_{xz}\\ \tau_{zx}\end{Bmatrix}=\begin{bmatrix}Q_{44} & 0\\ 0 & Q_{55}\end{bmatrix}\begin{Bmatrix}\gamma_{yz}\\ \gamma_{zx}\end{Bmatrix} \tag{8b}$$

where (σ_x, σ_y, τ_{xy}, τ_{yz}, and τ_{zx}) are the stress components, and (ε_x, ε_y, γ_{xy}, γ_{yz}, and γ_{zx}) are the corresponding strain components. The stiffness coefficients Q_{ij} can be expressed as

$$\begin{aligned} Q_{11}=Q_{22}&=\frac{E}{1-v^2},\\ Q_{12}&=\frac{vE}{1-v^2},\\ G=Q_{44}=Q_{55}=Q_{66}&=\frac{E}{2(1+v)}, \end{aligned} \tag{9}$$

2.3 Governing equations

The governing equilibrium equations can be derived using the virtual displacement principle. The principle of virtual work for this problem can be expressed as

$$\int_{-h/2}^{h/2}\int_{\Omega}\begin{bmatrix}\sigma_x\delta\varepsilon_x+\sigma_y\delta\varepsilon_y+\tau_{xy}\delta\gamma_{xy}+\tau_{yz}\delta\gamma_{yz}\\ +\tau_{xz}\delta\gamma_{xz}\end{bmatrix}d\Omega dz-\int_{\Omega}q\delta W d\Omega=0 \tag{10}$$

Where Ω represents the upper surface of the plate. By substituting Eqs. (5), (6), and (8) into Eq. (10) and integrating through the plate thickness, Eq. (10) can be rewritten as

$$\begin{aligned}\int_{\Omega}\ [&N_x\delta\varepsilon_x^0+N_y\delta\varepsilon_y^0+N_{xy}\delta\varepsilon_{xy}^0+M_x^b\delta k_y^b+M_y^b\delta k_y^b+M_{xy}^b\delta k_{xy}^b+M_x^s\delta k_x^s+M_y^s\delta k_y^s+\\ &M_{xy}^s\delta k_{xy}^s+S_{yz}^s\delta\gamma_{yz}^s+S_{xz}^s\delta\gamma_{yz}^s]d\Omega-\int_{\Omega}q(\delta w_b+\delta w_b)\,d\Omega=0\end{aligned} \tag{11}$$

The resulting forces N, M, and S are defined as

$$\begin{aligned}\left(N_x,N_y,N_{xy}\right)&=\int_{-h/2}^{h/2}\left(\sigma_x,\sigma_y,\tau_{xy}\right)dz\\ \left(M_x^b,M_y^b,M_{xy}^b\right)&=\int_{-h/2}^{h/2}\left(\sigma_x,\sigma_y,\tau_{xy}\right)zdz\\ \left(M_x^s,M_y^s,M_{xy}^s\right)&=\int_{-h/2}^{h/2}\left(\sigma_x,\sigma_y,\sigma_{xy}\right)fdz\\ \left(S_{xz}^s,S_{yz}^s\right)&=\int_{-h/2}^{h/2}\left(\tau_{xz},\tau_{yz}\right)gdz\end{aligned} \tag{12}$$

Substituting Eq. (8) into Eq. (12), the resulting forces are

$$\begin{Bmatrix}N\\ M^b\\ M^s\end{Bmatrix}=\begin{bmatrix}A & B & B^s\\ B & D & D^s\\ B^S & D^s & H^s\end{bmatrix}\begin{Bmatrix}\varepsilon\\ k^b\\ k^s\end{Bmatrix} \tag{13a}$$

$$\begin{Bmatrix}S_{yz}^s\\ S_{xz}^s\end{Bmatrix}=\begin{bmatrix}A_{44}^s & 0\\ 0 & A_{55}^s\end{bmatrix}\begin{Bmatrix}\gamma_{yz}^s\\ \gamma_{xz}^s\end{Bmatrix} \tag{13b}$$

$$N=\left\{N_x,N_y,N_{xy}\right\}^t, \tag{14a}$$

$$\varepsilon = \{\varepsilon_x^0, \varepsilon_y^0, \gamma_{xy}^0\}, k^b = \{k_x^b, k_y^b, k_{xy}^b\}, k^s = \{k_x^s, k_y^s, k_{xy}^s\}, \tag{14b}$$

Where

$$A = \begin{bmatrix} A_{11} & A_{12} & 0 \\ A_{12} & A_{22} & 0 \\ 0 & 0 & A_{66} \end{bmatrix}, B = \begin{bmatrix} B_{11} & B_{12} & 0 \\ B_{12} & B_{22} & 0 \\ 0 & 0 & B_{66} \end{bmatrix},$$
$$D = \begin{bmatrix} D_{11} & D_{12} & 0 \\ D_{12} & D_{22} & 0 \\ 0 & 0 & D_{66} \end{bmatrix}, B^s = \begin{bmatrix} B_{11}^s & B_{12}^s & 0 \\ B_{12}^s & B_{22}^s & 0 \\ 0 & 0 & B_{66}^s \end{bmatrix},$$
$$D^s = \begin{bmatrix} D_{11}^s & D_{12}^s & 0 \\ D_{12}^s & D_{22}^s & 0 \\ 0 & 0 & D_{66}^s \end{bmatrix}, H^s = \begin{bmatrix} H_{11}^s & H_{12}^s & 0 \\ H_{12}^s & H_{22}^s & 0 \\ 0 & 0 & H_{66}^s \end{bmatrix},$$

Where A_{ij}, B_{ij}, etc. are the plate stiffnesses, defined as

$$\{A_{ij}, B_{ij}, D_{ij}, E_{ij}, F_{ij}, H_{ij}\} = \sum_{n=1}^{3} \int_{h_n}^{h_{n+1}} \{1, z, z^2, z^3, z^4, z^6\} Q_{ij} dz, \qquad (i, j = 1,2,6)$$

$$B_{ij}^s = \frac{1}{4} B_{ij} + \frac{5}{3h^2} E_{ij}, \qquad (i, j = 1,2,6)$$

$$D_{ij}^s = \frac{1}{4} D_{ij} + \frac{5}{3h^2} F_{ij}, \qquad (i, j = 1,2,6)$$

$$H_{ij}^s = \frac{1}{16} D_{ij} - \frac{5}{6h^2} F_{ij} + \frac{25}{9h^4} H_{ij}, \qquad (i, j = 1,2,6)$$

$$\{A_{ij}, D_{ij}, F_{ij}\} = \sum_{n=1}^{3} \int_{h_n}^{h_{n+1}} \{1, z^2, z^4\} Q_{ij} dz, \qquad (i, j = 4,5)$$

$$A_{ij}^s = \frac{25}{16} A_{ij} - \frac{25}{6h^2} D_{ij} + \frac{25}{h^4} F_{ij}, \qquad (i, j = 4,5)$$

The governing equations can be derived from Eq. (11) by integrating the displacement gradients by parts and setting the coefficients δ_u, δ_v, δ_{wb}, and δ_{ws} to zero. This approach yields equilibrium equations associated with the current refined plate theory (RPT) for a metal foam rectangular plate.

$$\begin{gathered} \delta u: \frac{\partial N_x}{\partial x} + \frac{\partial N_{xy}}{\partial y} = 0 \\ \delta v: \frac{\partial N_{xy}}{\partial x} + \frac{\partial N_y}{\partial y} = 0 \\ \delta w_b: \frac{\partial^2 M_x^b}{\partial x^2} + 2\frac{\partial^2 M_{xy}^b}{\partial x\, \partial y} + \frac{\partial^2 M_y^b}{\partial y^2} + q = 0 \\ \delta w_s: \frac{\partial^2 M_x^s}{\partial x^2} + 2\frac{\partial^2 M_{xy}^s}{\partial x\, \partial y} + \frac{\partial^2 M_y^s}{\partial y^2} + \frac{\partial S_{xz}^s}{\partial x} + \frac{\partial S_{yz}^s}{\partial y} + q = 0 \end{gathered} \tag{15}$$

Substituting Eq. (13) into Eq. (15), we obtain

$$[L]\{\delta\} = \{f\}, \tag{16}$$

Where: The operators $\{\delta\} = \{u, v, w_b, w_s\}^t$, and $\{f\} = \{0, 0, q, q\}^t$ is the vector of generalized forces, and is the symmetric matrix of differential operators

$$\begin{gathered}
L_{11} = A_{11}d_{11} + A_{66}d_{22}, \\
L_{12} = (A_{12} + A_{66})d_{12}, \\
L_{13} = -B_{11}d_{111} - (B_{12} + 2B_{66})d_{122}, \\
L_{14} = -B^s_{11}d_{111} - (B^s_{12} + 2B^s_{66})d_{122}, \\
L_{22} = A_{22}d_{22} + A_{66}d_{11}, \\
L_{23} = -B_{22}d_{222} - (B_{12} + 2B_{66})d_{112}, \\
L_{24} = -B^s_{22}d_{222} - (B^s_{12} + 2B^s_{66})d_{112}, \\
L_{33} = D_{11}d_{1111} + 2(D_{12} + 2D_{66})d_{1122} + D_{22}d_{2222}, \\
L_{34} = D^s_{11}d_{1111} + 2(D^s_{12} + 2D^s_{66})d_{1122} + D^s_{22}d_{2222}, \\
L_{44} = H^s_{11}d_{1111} + 2(H^s_{12} + 2H^s_{66})d_{1122} + H^s_{22}d_{2222} - A^s_{55}d_{11} - A^s_{44}d_{22}.
\end{gathered} \tag{17}$$

where d_{ij} d_{ijl} and d_{ijlm} are the following differential operators

$$d_{ij} = \frac{\partial^2}{\partial x_i \partial x_j}, d_{ij} = \frac{\partial^3}{\partial x_i \partial x_j}, d_{ijlm} = \frac{\partial^4}{\partial x_i \partial x_j \partial x_l \partial x_m}, \quad (i, j, l, m = 1,2) \tag{18}$$

2.4 Analytical solutions for metal foam rectangular plates

The metal foam rectangular plates corresponded to the type of support used. Here, we focus on the analytical solutions of Eq. (16) for a supported metal foam rectangular plate. The following boundary conditions are imposed on the edges of the plate

$$v(0,y) = w_b(0,y) = w_s(0,y) = \frac{\partial w_b}{\partial y}(0,y) = \frac{\partial w_s}{\partial y}(0,y) = 0 \tag{19a}$$

$$v(a,y) = w_b(a,y) = w_s(a,y) = \frac{\partial w_b}{\partial y}(a,y) = \frac{\partial w_s}{\partial y}(a,y) = 0 \tag{19b}$$

$$N_x(0,y) = M^b_x(0,y) = M^s_x(0,y) = N_x(a,y) = M^b_x(a,y) = M^s_x(a,y) = 0 \tag{19c}$$

$$u(x,0) = w_b(x,0) = w_s(x,0) = \frac{\partial w_b}{\partial x}(x,0) = \frac{\partial w_s}{\partial x}(x,0) = 0 \tag{19d}$$

$$u(x,b) = w_b(x,b) = w_s(x,b) = \frac{\partial w_b}{\partial x}(x,b) = \frac{\partial w_s}{\partial x}(x,b) = 0 \tag{19e}$$

$$N_y(x,0) = M^b_y(x,0) = M^s_y(x,0) = N_y(x,b) = M^b_y(x,b) = M^s_y(x,b) = 0 \tag{19f}$$

In the Navier solution, the following solution form is assumed, which must satisfy the imposed boundary conditions

$$\begin{Bmatrix} u \\ v \\ w_b \\ w_s \end{Bmatrix} = \begin{Bmatrix} \bar{U}\cos(\lambda x)\sin(\mu y) \\ \bar{V}\sin(\lambda x)\cos(\mu y) \\ \bar{W}_b\sin(\lambda x)\sin(\mu y) \\ \bar{W}_s\sin(\lambda x)\sin(\lambda y) \end{Bmatrix} \tag{20}$$

where $\bar{U}, \bar{V}, \bar{W}_b$ and , $\bar{W}_s$ are the parameters determined by satisfying the conditions of Eq. (20) and

the governing Eq. (16).

To solve this problem, Navier introduced an external force for the case of a sinusoidal load as follows

$$q(x,y) = q_0\, sin(\lambda x)\, sin(\mu y), \tag{21}$$

where $\lambda = \pi/a$ and $\mu = \pi/b$, and q_0 represents the intensity of the load at the center of the plate.

This leads to the following operator equation

$$[K]\{\Delta\} = \{F\} \tag{22}$$

Where $\{\Delta\}$ et $\{F\}$ are column vectors and $[K]$ is the symmetric matrix given by

$$\{\Delta\} = \{\bar{U}, \bar{V}, \bar{W}_b, \bar{W}_s\}\,, \quad \{F\} = \{0,0,q_0,q_0\}. \tag{23}$$

$$[K] = \begin{bmatrix} a_{11} & a_{12} & a_{13} & a_{14} \\ a_{12} & a_{22} & a_{23} & a_{24} \\ a_{13} & a_{23} & a_{33} & a_{34} \\ a_{14} & a_{24} & a_{34} & a_{44} \end{bmatrix} \tag{24}$$

Where

$$\begin{gathered} a_{11} = A_{11}\lambda^2 + A_{66}\mu^2; \\ a_{12} = \lambda\mu(A_{12} + A_{66}); \\ a_{13} = -\lambda[B_{11}\lambda^2 + (B_{12} + 2B_{66})\mu^2] \\ a_{14} = -\lambda[B_{11}^s\lambda^2 + (B_{12}^s + 2B_{66}^s)\mu^2]; \\ a_{22} = A_{66}\lambda^2 + A_{22}\mu^2; \\ a_{23} = -\mu[(B_{12} + 2B_{66})\lambda^2 + B_{22}\mu^2] \\ a_{24} = -\mu[(B_{12}^s + 2B_{66}^s)\lambda^2 + B_{22}^s\mu^2]; \\ a_{33} = D_{11}\lambda^4 + 2(D_{12} + 2D_{66})\lambda^2\mu^2 + D_{22}\mu^4 \\ a_{34} = D_{11}^S\lambda^4 + 2(D_{12}^s + 2D_{66}^s)\lambda^2\mu^2 + D_{22}^s\mu^4; \\ a_{44} = H_{11}^s\lambda^4 + 2(H_{11}^s + 2H_{66}^s)\lambda^2\mu^2 + H_{22}^s\mu^4 \quad + A_{55}^s\lambda^2 + A_{44}^s\mu^2 \end{gathered} \tag{25}$$

3. Results and discussion

In this study, the material parameters of the metal foam plate are as follows:

Young's modulus (E=200 GPa) and Poisson's ratio (ν=0.3)

The numerical results are presented in terms of the dimensionless deflection and stress. The variations in the dimensionless parameters used are as follows

Central Deflection: $$\bar{w} = \frac{10h^3E}{q_0a^4} w\left(\frac{a}{2}, \frac{b}{2}\right). \tag{26}$$

Axial Stress: $$\bar{\sigma}_{xx} = \frac{h}{q_0a}\sigma_{xx}\left(\frac{a}{2}, \frac{b}{2}, \frac{h}{2}\right) \quad \bar{\sigma}_{yy} = \frac{h}{q_0a}\sigma_{yy}\left(\frac{a}{2}, \frac{b}{2}, \frac{h}{3}\right) \tag{27}$$

Shear Stress: $$\bar{\tau}_{xz} = \frac{h}{q_0a}\tau_{xz}\left(0, \frac{b}{2}, 0\right),$$

Table 1 Non-dimensional deflection, normal, and tangential stresses for the metal foam plate subjected to sinusoidal load ($a=b$ and a/h=10)

Theory	$\overline{w}$	$\bar{\sigma}_x$	$\bar{\sigma}_y$	$\bar{\tau}_{yz}$	$\bar{\tau}_{xz}$	$\bar{\tau}_{xy}$
Nebab *et al.* (2019)	0.29603	1.99550	-	-	0.24618	0.70652
Himeur *et al.* (2022)	0.29605	1.99472	-	-	0.24193	0.70662
Zenkour and Radwan (2020)	0.2960	1.9966	1.3119	0.2134	0.2538	0.7064
Wang and Zhang (2019)	0.2961	1.9943	1.3124	0.2121	0.2386	0.7067
Present	0.296056	1.99432	1.31237	0.212064	0.238572	0.706655

Table 2 Comparison of the non-dimensional deflections and transverse shear stresses in a square isotropic plate subjected to sinusoidally distributed load

a/h	wE/q_0h			$\tau_{xz}(0,b/2)/q_0$		
	Matsunaga (2009)	Mechab *et al.* (2010)	Present	Matsunaga (2009)	Mechab *et al.* (2010)	Present
5	0.2098	0.2146	0.21457	0.1186	0.1190	0.11904
10	0.2943	0.2961	0.29605	0.2383	0.2385	0.23857

$$\bar{\tau}_{xy} = \frac{h}{q_0 a}\tau_{xy}\left(0,0,-\frac{h}{3}\right), \quad \bar{\tau}_{yz} = \frac{h}{q_0 a}\tau_{yz}\left(\frac{a}{2},0,\frac{h}{6}\right) \tag{28}$$

To establish the viability of the relevant theory, the results obtained for rectangular plates made of metal foam were compared with previously reported results (Himeur *et al.* 2022, Nebab *et al.* 2019, Wang and Zhang 2019, Zenkour and Radwan 2020). For verification, rectangular plates with foam were investigated using existing theories in the literature, such as the Higher-Order Shear Deformation Plate Theory (HSDPT), refined higher-order plate theory (RPT), and Sinusoidal Shear Deformation Plate Theory (SSDPT). The performance of these models is presented in Table 1.

The present study shows close agreement with both Wang and Zhang (2019), Nebab *et al.* (2019), thus displaying differences in the central deflection of less than 0.02%. This correspondence reinforces the RPT's capability to accurately predict the deformation of a plate under applied loads. The axial stress values obtained from the RPT showed excellent agreement with the values of axial stress obtained in Zenkour and Radwan (2020), Wang and Zhang (2019), with discrepancies below 0.01%. This signifies the efficient capture of the stress distribution in the plate by the RPT. The shear stress derived from the RPT closely corresponded with the results of Wang and Zhang (2019), Zenkour and Radwan (2020), deviating by less than 0.01%. This reinforces the capacity of the RPT to accurately predict the shear forces acting on the plate.

The present study compared its findings with those of (Himeur *et al.* 2022, Nebab *et al.* 2019, Wang and Zhang 2019), While these studies use technologically oriented procedures, namely, less than 0.1% differences in any of the parameters, they should reiterate the consistent results gained in the papers and strengthen their basis further.

Minor numerical discrepancies may be caused by numerical accuracy, slight variations in the implementation of the theories, or rounding errors during calculations. The matching of the present study results to established theories demonstrates the robustness of the proposed RPT, which shows that it can consistently provide correct results in analyzing the behavior of metal foam

rectangular plates.

Table 2 demonstrates excellent agreement between the present analytical method and the established literature Matsunaga (2009), Mechab *et al*. (2010) for both the non-dimensional deflection and transverse shear stress in square isotropic plates under sinusoidal loading. The close numerical correspondence across different thickness ratios (a/h=5 and 10) validates the accuracy of the proposed theoretical approach. These consistent results confirm the reliability of the adopted methodology for analyzing the plate bending and shear behavior under distributed loads.

The analysis shown in Figs. 2 and 3 reveals complex relationships between the plate geometry, thickness, and deflection behavior under sinusoidal loading.

Fig. 2 illustrates the variation of the dimensionless deflection (w) with respect to the thickness ratio (a/h) for rectangular Metal Foam plates under sinusoidal mechanical loading. The graph shows multiple curves representing different geometric ratios (a/b).

The curves exhibit a linear decrease in deflection as a/h increases up to a critical value of a/h=8. Beyond this point, the deflection remained relatively constant, indicating a transition in the plate behavior. The linear decrease in the initial portion of the curves (a/h<8) can be attributed to the increasing plate stiffness as the thickness increased relative to the planar dimensions. This behavior aligns with the classical plate theory, where deflection is inversely proportional to the cube of the thickness. However, the transition to a constant deflection at a/h=8 suggests a limit to this relationship, possibly due to the increasing influence of shear deformation effects in thicker plates.

The analysis of the curves from $a=b$ to $a=0.125b$ revealed a progressive increase in the deflection magnitude, which correlated with the changes in the plate aspect ratio. The square plate ($a=b$) exhibited the lowest deflection values, indicating the stiffest configuration owing to the balanced stiffness in both planar directions. As the aspect ratio changes, the deflection increases: $a=2b$ shows a slightly higher deflection than the square plate ($a=b$) owing to the reduced stiffness from the increased length in one direction. The $a=0.25b$ configuration demonstrated significantly higher deflection, with the wider, shorter geometry resulting in reduced stiffness in the shorter direction. The $a=0.125b$ case exhibited the highest deflection values, representing the least stiff configuration among those presented. This trend of increasing deflection from $a=b$ to $a=0.125b$ is attributed to the change in the plate aspect ratio. As the plate widens relative to its length (decreasing a/b ratio), its behavior shifts towards that of a beam in the shorter direction, leading to increased deflection under identical loading conditions.

The constant deflection beyond a/h=8 for all geometric ratios is particularly intriguing. This phenomenon suggests a limit to the stiffening effect of increasing thickness, possibly due to the following:

- Shear deformation effects dominate thicker plates, which are not considered in classical thin plate theory.

Beyond the thickness ratio, sinusoidal loading affects only the surface layers of the plate, with deeper layers contributing minimally to the overall deflection.

Fig. 3 depicts the relationship between the dimensionless central deflection (w) and the geometric ratio (b/a) for Metal Foam plates under sinusoidal loading, with curves representing different thickness ratios (a/h). The curves exhibit a linear increase in deflection as the b/a ratio increases, indicating a direct correlation between the plate aspect ratio and deflection magnitude.

The increasing linear deflection (w) due to the increased plate length-to-width ratio aligns with the classical plate theory, which states that bent plates under transverse loads become comparatively longer. As the b/a ratio increases, the stiffness of the plate decreases longitudinally,

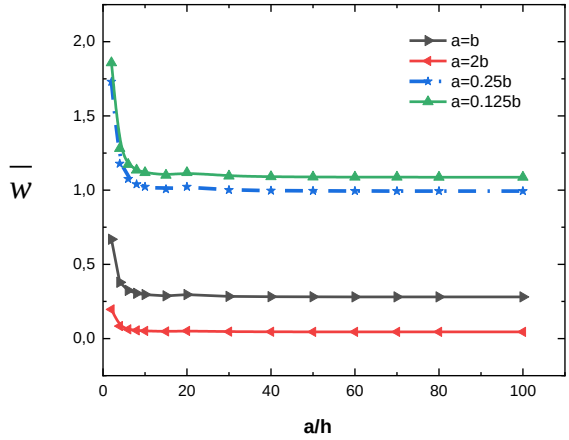

Fig. 2 The non-dimensional deflection metal foam rectangular plates subjected to sinusoidal mechanical loads vary with the thickness ratio *a/h* (η=0.8058)

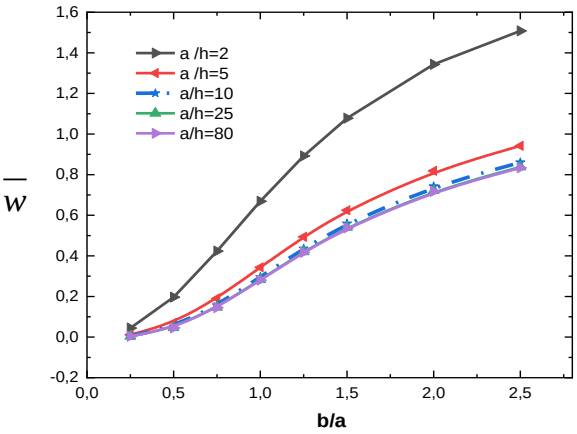

Fig. 3 Dimensionless deflection concerning geometric ratio (*b/a*) of the metal foam plate for different thickness ratios under a sinusoidal load (η=0.8713)

therefore, we observe higher deflection values.

There was substantial convergence. The deflections are similar in all cases for *b/a*=0.25, regardless of the *a/h* ratio. This can be interpreted as a unique geometric configuration in which the plate behavior is largely determined by the aspect ratio of the plate, with the thickness effects neglected.

Subsequently, with an increase in *b/a*, the curves diverge, and the thinner plates (lower *a/h*) are subjected to a greater enhancement of deflection than other plates owing to the dominating bending effects.

For thinner plates with lower (*a/h*) ratios, the deflections are more significant for all *b/a* ratios, the deflection value from the curve with *a/h*=2 is significantly different than that using *a/h*=80. The rates of increase in deflection with respect to *b/a* are more significant for thinner plates, as indicated by the steep slopes of the curves with smaller a/h ratios. Conversely, in the cases of higher thickness ratios, as *a/h* increases, the curves flatten out, thereby suggesting that the

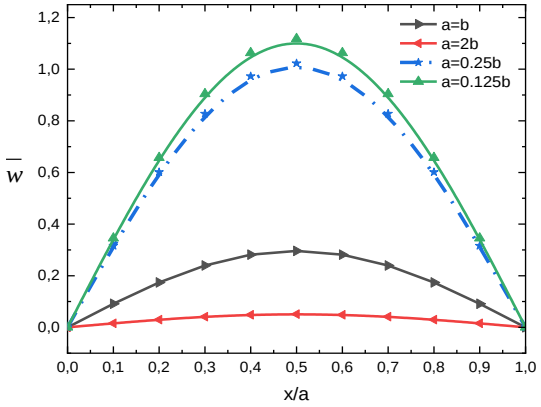

Fig. 4 The variation in the non-dimensional deflexion relates to the plate length (a/h=10) for different metal foam plate geometric ratios (η=0.6012)

deflection that changes with b/a reduces the thickness. The effect of the b/a ratio is very pronounced between 0 and 1, thereafter, there is a slowdown in the rate of increase in deflection for any a/h ratio.

The discrepancies among the curves for various a/h ratios were attributed to the differences in the contributions of bending and shear deformation to the overall plate response. Bending dominates thinner plates with low a/h ratios, leading to more significant deflection and higher sensitivity to aspect ratio changes. As the plate thickness increases or at high a/h ratios, shear deformation contributes more significantly, leading to lower overall deflection and, hence, less sensitivity to changes in the aspect ratio (Mechab *et al*. 2010).

Fig. 4 shows the variation in the dimensionless deflection along the x-direction of the plate for different geometric ratios (a/b) at a thickness ratio of a/h=10. The deflection profile exhibited symmetry about the plate center, with the maximum deflection occurring at the midpoint (x/a=0.5) for all geometric configurations. This symmetry is expected because of the supported boundary conditions and sinusoidal loading. The results demonstrate the influence of the plate aspect ratio on the deflection magnitude and its distribution. The overall deflection decreases as the plate becomes more elongated in the x-direction (increasing the a/b ratio). The highest deflections were observed for the flattest plate configuration (a=0.125b), whereas the lowest deflections were observed for the most elongated plate (a=2b). This trend can be attributed to the increased stiffness in the longer direction as the plate decelerated. The deflection curves for intermediate aspect ratios (a=0.25b and a=b) fell between these extremes, forming an envelope of deflection profiles. The shapes of the deflection curves remained similar across all aspect ratios, indicating that the fundamental deformation mode was consistent, but the geometric configuration scaled the magnitude.

This study used a refined plate theory to examine the flexural behavior of supported Metal Foam rectangular plates under sinusoidal mechanical loading. Figs. 5-8 illustrate the distribution of the dimensionless normal stress (σ_{xx} and σ_{yy}) across the plate thickness for various geometric ratios (b/a and a/h).

Fig. 5 shows that for a fixed aspect ratio (b/a), increasing the thickness-to-side ratio (a/h) reduces the magnitude of σ_{xx}, indicating a decrease in bending stress with increasing plate thickness. This trend is consistent across different aspect ratios, as shown in Fig. 6, where σ_{xx} is

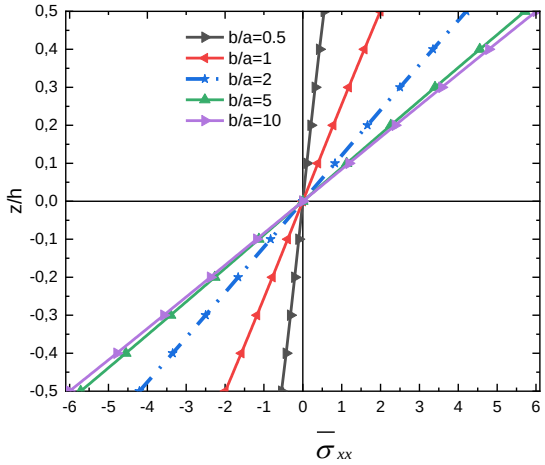

Fig. 5 The variation of dimensionless normal stress relative to plate thickness (a/h=10) under sinusoidal loads for different geometric ratios (η=0.8058)

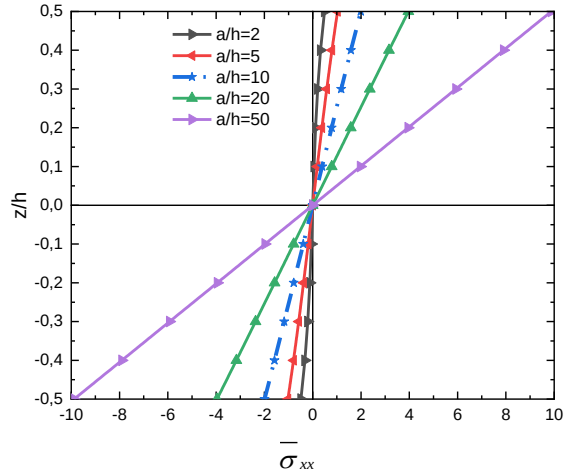

Fig. 6 The variation of dimensionless normal stress concerning the thickness of a metal foam square plate (b/a=1) under a sinusoidal load for different thickness ratios (a/h) (η=0.8713)

plotted against z/h for a square plate (b/a=1) with varying a/h. Similarly, Fig. 5 illustrates the variation in the dimensionless normal stress σ_{xx} across the thickness of a Metal Foam plate (a/h=10) under sinusoidal load for different geometric ratios (b/a). The results show that the geometric ratio significantly affects the normal stress distribution. For all b/a ratios, the stress distribution was antisymmetric about the mid-plane of the plate, with tensile stresses on the upper surface and compressive stresses on the lower surface. This behavior is consistent with the classical plate bending theory. As the b/a ratio increases from 0.5 to 10, the magnitude of the stresses at the surface decreases, indicating that plates with higher b/a ratios (more elongated in the y-direction) experience lower bending stresses for the same applied load. This trend is consistent across different aspect ratios, as shown in Fig. 6, where σ_{xx} is plotted against z/h for a square plate (b/a=1) with varying a/h. Similarly, as the a/h ratio increased (i.e., the plate became thinner), the

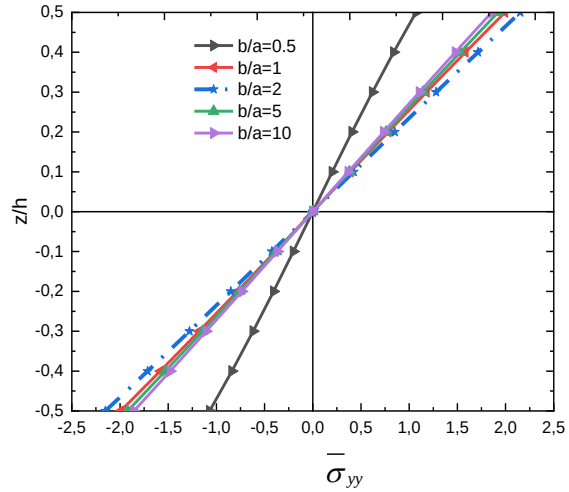

Fig. 7 The variation of dimensionless normal stress relative to plate thickness (a/h=10) under sinusoidal loads for different geometric ratios (η=0.8058)

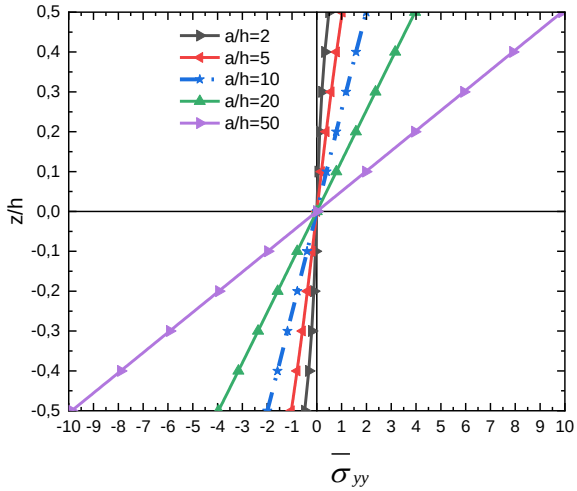

Fig. 8 The variation of dimensionless normal stress concerning the thickness of a metal foam square plate (b/a=1) under a sinusoidal load for different thickness ratios (a/h) (η=0.8713)

stress gradients near the surfaces became steeper, and the overall stress magnitude increased. This behavior was expected because thinner plates experience higher bending stresses for the same applied load. The stress distribution remained antisymmetric for all thickness ratios, consistent with the bending behavior of the Metal Foam plates.

Fig. 6 illustrates the variation in the dimensionless normal stress σ_{yy} across the thickness of a square Metal Foam plate (b/a=1) for different thickness ratios (a/h). The trends observed were similar, with stress gradients becoming steeper and overall stress magnitudes increasing as the plate became thinner (higher a/h ratios). However, the magnitudes of σ_{yy} stresses are generally lower than σ_{xx} stresses for the same thickness ratios, particularly for thicker plates (lower a/h ratios). This difference diminishes as the plate becomes very thin (a/h=50), suggesting that the

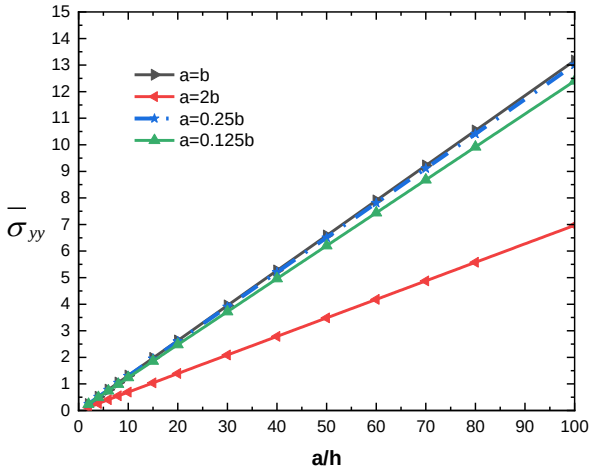

Fig. 9 Variation of dimensionless normal stress concerning the metal foam plate's thickness (a/h) under sinusoidal load for different geometric ratios (η=0.6012)

stress distribution of extremely thin plates becomes more uniform in both directions.

Similarly, Figs. 7 and 8 depict the variation in σ_{yy}, which shows a trend similar to that of σ_{xx}. The magnitude of σ_{yy} decreased with increasing a/h, highlighting the influence of plate thickness on the stress distribution. Fig. 7 shows the variation in the dimensionless normal stress σ_{yy} across the thickness of a Metal Foam plate (a/h=10) for different geometric ratios (b/a). Similar to Fig. 5, the stress distribution was antisymmetric about the midplane. However, the magnitude of σ_{yy} stress is generally lower than that of σ_{xx} stress at the same geometric ratio. As the b/a ratio increases, the magnitude of σ_{yy} stress decreases more rapidly than that of σ_{xx} stress. This difference can be attributed to the plate geometry and loading conditions, where the stress distribution in the y-direction is more sensitive to changes in the b/a ratio.

The results presented in Fig. 9 illustrate the variation of dimensionless normal stress σ_{yy} with respect to the thickness ratio (a/h) for a Metal Foam rectangular plate subjected to sinusoidal loading. The graph demonstrates the significant influence of the thickness and geometric ratios on the normal stress distribution. As the thickness ratio (a/h) increases, indicating a transition from thick to thin plates, the dimensionless normal stress σ_{yy} exhibits a consistent increasing trend for all geometric ratios. This behavior aligns with the classical plate theory, which predicts higher bending stresses in thinner plates under the same loading conditions. This trend can be attributed to the increased stiffness of the thicker plates, which led to a more concentrated stress distribution. The effect of the geometric ratio (a/b) on the stress distribution is also evident, with different curves representing various plate aspect ratios. The plate with a=0.125b (most elongated in the y-direction) exhibited the highest stress values, followed by a=0.25b, a=b (square plate), and a=2b (elongated in the x-direction). This ordering suggests that plates with smaller width-to-length ratios (more elongated in the y-direction) experience higher normal stresses in the y-direction under given loading conditions. The stress amplification is particularly pronounced for very thin plates (high a/h ratios), where the curves show a steep increase.

Fig. 10 illustrates the variation of dimensionless transverse shear stress σ_{xz} through the thickness of a square Metal Foam plate (a/b=1) for different thickness ratios (a/h). The results revealed that the maximum transverse shear stress consistently occurred at the neutral axis (z=0)

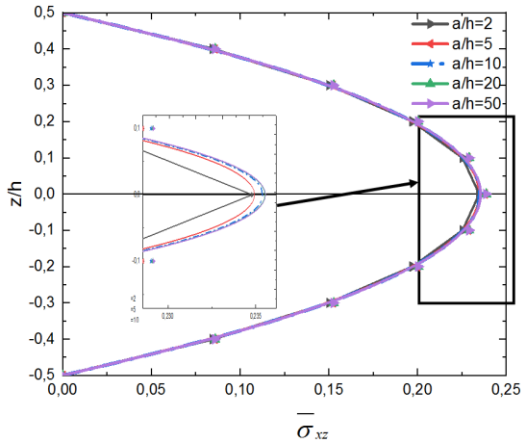

Fig. 10 Variation of the dimensionless transverse shear stress for different thickness ratios (a/h=10) of metal foam square plates subjected to sinusoidal loads (η=0.8058)

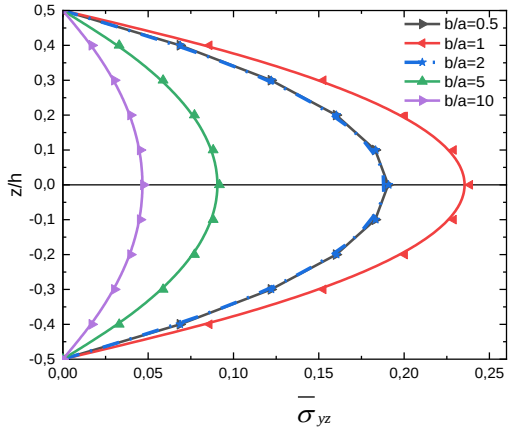

Fig. 11 Variation of the dimensionless transverse shear stress for different thickness ratios (a/h=10) of metal foam square plates subjected to sinusoidal loads (η=0.6012)

for all thickness ratios, which aligned with the classical plate theory predictions. Interestingly, the effect of the thickness ratio on the shear stress distribution appears to be minimal in this case, as the curves for different a/h ratios nearly overlap. This observation suggests that the refined plate theory used in this study captures a relatively consistent shear stress profile across various plate thicknesses for the square plates. However, it is worth noting that this behavior might differ from some higher-order shear deformation theories that often predict more pronounced thickness effects on transverse shear stresses. The symmetry of the stress distribution about the neutral axis was consistent with the expected behavior of Metal Foam materials under symmetric loading conditions.

Fig. 11 presents the variation of dimensionless transverse shear stress σ_{yz} through the thickness of rectangular Metal Foam plates with different geometric ratios (b/a) at a fixed thickness ratio (a/h=10). The results demonstrated a significant influence of the geometric ratio on the transverse shear stress distribution. Similar to Fig. 10, the maximum shear stress occurred at the neutral axis

(z=0) for all geometric ratios. However, the magnitude of the shear stress varied considerably with the b/a ratio. The square plate (b/a=1) exhibited the highest maximum shear stress, whereas plates with b/a ratios deviating from unity (both larger and smaller) showed reduced shear stress magnitudes. This indicates that square plates may be more susceptible to transverse shear deformations than rectangular plates under similar loading conditions. This trend can be attributed to the interaction between the aspect ratio of the plate and the sinusoidal loading pattern, which may lead to more complex stress states in square plates. Additionally, the stress distributions remained symmetric about the neutral axis for all geometric ratios, confirming the consistency of the refined plate theory in capturing the Metal Foam material behavior.

4. Conclusions

This study advances the understanding of the mechanical behavior of supported rectangular Metal Foam plates by applying a refined four-variable plate theory. This investigation focused on the effects of geometric parameters and sinusoidal loading on plate deflection and stress distribution, addressing a significant gap in the literature. A semi-analytical approach that combines the principle of virtual work with Navier's solution method achieved a robust analysis of plate mechanics under various conditions.

The results illuminate the complex relationships between the plate geometry, thickness ratios, and deflection behavior. One significant finding for plate design considerations is the critical thickness ratio at which the plate behavior transitions (a/h=8). These include the analysis of different aspect ratios in plates that transition from square to asymmetrical shapes (a=0.125b) to gain insight into the effect of geometry on the plate stiffness and deflection patterns.

The validation of the proposed refined plate theory against established higher-order shear deformation theories showed excellent agreement. A comparison with other studies showed minor discrepancies (Himeur *et al.* 2022, Nebab *et al.* 2019, Wang and Zhang 2019, Zenkour and Radwan 2020) which hardly exceeded 0.1% for all parameters, thus confirming its robustness.

A long line of hidden engineering considerations and implications will benefit industries dealing with aerospace, automotive, and similar applications, where modeling and correct predictions of plates and their responses remain paramount. An overview of this research provides engineers and designers with an in-depth understanding of how various geometric specifications and loading conditions affect plate performance.

Although this represents a significant improvement in plate theory, it opens up avenues for future investigations. Areas for further research include applying this refined theory to more complex loading arrangements, non-metal foam materials, and dynamic loading conditions.

References

Addou, F.Y., Bourada, F., Meradjah, M., Bousahla, A.A., Tounsi, A., Ghazwani, M.H. and Alnujaie, A. (2023), "Impact of porosity distribution on static behavior of functionally graded plates using a simple quasi-3D HSDT", *Comput. Concrete*, **32**(1), 87-97. https://doi.org/10.12989/cac.2023.32.1.087.

Adhikari, B., Dash, P. and Singh, B. (2020), "Buckling analysis of porous FGM sandwich plates under various types nonuniform edge compression based on higher order shear deformation theory", *Compos. Struct.*, **251**, 112597. https://doi.org/10.1016/j.compstruct.2020.112597.

Aktarer, S.M., Kucukomeroglu, T., Sekban, D.M., Yaylaci, E.U., Yaylaci, M., Ozdemir, M.E. and

Mirzaloglu, I. (2025), "Analysis of the changes in microstructure, mechanical, and contact properties of multi-pass friction stir processed DP800 steel", *Adv. Nano Res.*, **18**(3), 253-264. https://doi.org/10.12989/anr.2025.18.3.253.

Ansari, R., Hasrati, E., Shojaei, M.F., Gholami, R. and Shahabodini, A. (2015), "Forced vibration analysis of functionally graded carbon nanotube-reinforced composite plates using a numerical strategy", *Physica E: Low Dimens. Syst. Nanostr.*, **69**, 294-305. https://doi.org/10.1016/j.physe.2015.01.011.

Bentrar, H., Chorfi, S.M., Belalia, S.A., Tounsi, A., Ghazwani, M.H. and Alnujaie, A. (2023), "Effect of porosity distribution on free vibration of functionally graded sandwich plate using the P-version of the finite element method", *Struct. Eng. Mech.*, **88**(6), 551-567. https://doi.org/10.12989/sem.2023.88.6.551.

Berkia, A., Benguediab, S., Menasria, A., Bouhadra, A., Bourada, F., Mamen, B., ... & Hussain, M. (2022), "Static buckling analysis of bi-directional functionally graded sandwich (BFGSW) beams with two different boundary conditions", *Steel Compos. Struct.*, **44**(4), 503-517. https://doi.org/10.12989/scs.2022.44.4.503.

Chen, D., Yang, J. and Kitipornchai, S. (2016), "Free and forced vibrations of shear deformable functionally graded porous beams", *Int. J. Mech. Sci.*, **108**, 14-22. https://doi.org/10.1016/j.ijmecsci.2016.01.025.

Chen, D., Yang, J. and Kitipornchai, S. (2017), "Nonlinear vibration and postbuckling of functionally graded graphene reinforced porous nanocomposite beams", *Compos. Sci. Technol.*, **142**, 235-245. https://doi.org/10.1016/j.compscitech.2017.02.008.

Chen, D., Yang, J. and Kitipornchai, S. (2019), "Buckling and bending analyses of a novel functionally graded porous plate using Chebyshev-Ritz method", *Arch. Civil Mech. Eng.*, **19**(1), 157-170. https://doi.org/10.1016/j.acme.2018.09.004.

Driz, H., Attia, A., Bousahla, A.A., Addou, F.Y., Bourada, M., Tounsi, A., Tounsi, A., Balubaid, M. and Mahmoud, S. (2024), "Dynamic response of imperfect functionally graded plates: Impact of graded patterns and viscoelastic foundation", *Struct. Eng. Mech.*, **91**(6), 551-565. https://doi.org/10.12989/sem.2024.91.6.551.

Dung, N.T., Minh, P.V., Hung, H.M. and Tien, D.M. (2021), "The third-order shear deformation theory for modeling the static bending and dynamic responses of piezoelectric bidirectional functionally graded plates", *Adv. Mater. Sci. Eng.*, **2021**(1), 5520240. https://doi.org/10.1155/2021/5520240.

Fuyad, S.T.M., Al Bari, M.A., Makfidunnabi, M., Nain, H.Z., Özdemir, M.E. and Yaylacı, M. (2024), "Finite element analysis of ratcheting on beam under bending-bending loading conditions", *Struct. Eng. Mech.*, **89**(1), 23-31. https://doi.org/10.12989/sem.2024.89.1.023.

Garg, A. and Chalak, H. (2019), "A review on analysis of laminated composite and sandwich structures under hygrothermal conditions", *Thin Wall. Struct.*, **142**, 205-226. https://doi.org/10.1016/j.tws.2019.05.005.

Garg, A., Chalak, H., Li, L., Belarbi, M.O., Sahoo, R. and Mukhopadhyay, T. (2022), "Vibration and buckling analyses of sandwich plates containing functionally graded metal foam core", *Acta Mechanica Solida Sinica*, **35**(4), 1-16. https://doi.org/10.1007/s10338-021-00295-z.

Gawah, Q., Al-Osta, M.A., Abdullah, M.A., Bourada, F., Tounsi, A., Ahmad, S., Al-Dulaijan, S.U. and Al-Zahrani, M.M. (2025), "Wave propagation analysis of graphene platelet-reinforced functionally graded porous plates resting on viscoelastic foundations using an integral HSDT", *Thin Wall. Struct.*, **215**, 113502. https://doi.org/10.1016/j.tws.2025.113502.

Himeur, N., Mamen, B., Benguediab, S., Bouhadra, A., Menasria, A., Bouchouicha, B., Bourada, F. and Benguediab, M. (2022), "Coupled effect of variable Winkler–Pasternak foundations on bending behavior of FG plates exposed to several types of loading", *Steel Compos. Struct.*, **44**(3), 353-369. https://doi.org/10.12989/scs.2022.44.3.353.

Hu, Z., Shi, Y., Guo, C., Du, J. and Li, R. (2024), "New analytical solutions for free vibration of cracked functionally graded rectangular plates", *AIAA J.*, **62**(10), 3960-3977. https://doi.org/10.2514/1.J063936.

Hu, Z., Zhou, C., Zheng, X., Ni, Z. and Li, R. (2023), "Free vibration of non-Lévy-type functionally graded doubly curved shallow shells: New analytic solutions", *Compos. Struct.*, **304**, 116389. https://doi.org/10.1016/j.compstruct.2022.116389.

Kaddari, M., Balubaid, M., Mahmoud, S., Kaci, A., Bousahla, A.A., Tounsi, A., Al-Osta, M.A. and Tounsi,

A. (2025), "Influence of porosity distribution on buckling behavior of FG sandwich plates using a quasi-3D refined plate theory", *Mech. Bas. Des. Struct. Mach.*, **53**(5), 3635-3662. https://doi.org/10.1080/15397734.2024.2434552.

Kadiri, A., Bendaida, M., Attia, A., Balubaid, M., Mahmoud, S., Bousahla, A.A., Tounsi, A., Bourada, F. and Tounsi, A. (2024), "Wave propagation in FG polymer composite nanoplates embedded in variable elastic medium", *Adv. Nano Res.*, **17**(3), 235-248. https://doi.org/10.12989/anr.2024.17.3.235.

Kar, V.R., Mahapatra, T.R. and Panda, S.K. (2015), "Nonlinear flexural analysis of laminated composite flat panel under hygro-thermo-mechanical loading", *Steel Compos. Struct.*, **19**(4), 1011-1033. https://doi.org/10.12989/scs.2015.19.4.1011.

Lakhdar, K., Sadoun, M., Addou, F.Y., Bourada, F., Bousahla, A.A., Tounsi, A., Khedher, K.M. and Tounsi, A. (2024), "Free vibrational characteristics of various imperfect FG beam via a novel integral Timoshenko's theory", *Acta Mechanica*, **235**(10), 6287-6304. https://doi.org/10.1007/s00707-024-04046-2.

Lakhdar, Z., Chorfi, S.M., Belalia, S.A., Khedher, K.M., Alluqmani, A.E., Tounsi, A. and Yaylacı, M. (2024), "Free vibration and bending analysis of porous bi-directional FGM sandwich shell using a TSDT p-version finite element method", *Acta Mechanica*, **235**(6), 3657-3686. https://doi.org/10.1007/s00707-024-03909-y.

Mantari, J., Oktem, A. and Soares, C.G. (2012), "A new higher order shear deformation theory for sandwich and composite laminated plates", *Compos. Part B: Eng.*, **43**(3), 1489-1499. https://doi.org/10.1016/j.compositesb.2011.07.017.

Matsunaga, H. (2009), "Stress analysis of functionally graded plates subjected to thermal and mechanical loadings", *Compos. Struct.*, **87**(4), 344-357. https://doi.org/10.1016/j.compstruct.2008.02.002.

Mechab, I., Atmane, H.A., Tounsi, A., Belhadj, H.A. and Bedia, E.A.A. (2010), "A two variable refined plate theory for the bending analysis of functionally graded plates", *Acta Mechanica Sinica*, **26**(6), 941-949. https://doi.org/10.1007/s10409-010-0372-1.

Menasria, A., Tamrabet, A., Bouhadra, A., Refrafi, S., Alselami, N.A., Mamen, B. and Tounsi, A. (2024), "Nonlinear temperature dependent and visco-elastic foundation effects on the free vibration of functionally graded sandwich plates with ceramic foam core", *J. Strain Anal. Eng. Des.*, **59**(8), 542-558. https://doi.org/10.1177/03093247241273834.

Messaoudi, A., Bouhadra, A., Menasria, A., Mamen, B., Boucham, B., Benguediab, M., Tounsi, A. and Al-Osta, M. (2023), "Impact of the shear and thickness stretching effects on the free vibrations of advanced composite plates", *Mech. Compos. Mater.*, **59**(5), 1001-1018. https://doi.org/10.1007/s11029-023-10148-0.

Mudhaffar, I.M., Chikh, A., Tounsi, A., Al-Osta, M.A., Al-Zahrani, M.M. and Al-Dulaijan, S.U. (2023), "Impact of viscoelastic foundation on bending behavior of FG plate subjected to hygro-thermo-mechanical loads", *Struct. Eng. Mech.*, **86**(2), 167-180. https://doi.org/10.12989/sem.2023.86.2.167.

Nebab, M., Ait Atmane, H., Bennai, R. and Tounsi, A. (2019), "Effect of variable elastic foundations on static behavior of functionally graded plates using sinusoidal shear deformation", *Arab. J. Geosci.*, **12**(24), 809. https://doi.org/10.1007/s12517-019-4871-5.

Nguyen, N.V., Nguyen, H.X., Lee, S. and Nguyen-Xuan, H. (2018), "Geometrically nonlinear polygonal finite element analysis of functionally graded porous plates", *Adv. Eng. Softw.*, **126**, 110-126. https://doi.org/10.1016/j.advengsoft.2018.11.005.

Nguyen, T.N., Thai, C.H., Luu, A.T., Nguyen-Xuan, H. and Lee, J. (2019), "NURBS-based postbuckling analysis of functionally graded carbon nanotube-reinforced composite shells", *Comput. Meth. Appl. Mech. Eng.*, **347**, 983-1003. https://doi.org/10.1016/j.cma.2019.01.011.

Öner, E., Yaylacı, E.U. and Yaylacı, M. (2024), "Multi-method examination of contact mechanics in orthotropic layers under gravity", *Mech. Mater.*, **195**, 105036. https://doi.org/10.1016/j.mechmat.2024.105036.

Rajendran, S., Loganathan, R., Yaylaci, M., Yaylaci, E.U. and Ozdemir, M.E. (2024), "Vibration of piezo-magneto-thermoelastic FG nanobeam submerged in fluid with variable nonlocal parameter", *Adv. Nano Res.*, **16**(5), 489-500. https://doi.org/10.12989/anr.2024.16.5.489.

Sekban, D.M., Yaylaci, E.U., Ozdemir, M.E. and Yaylaci, M. (2024), "Determination of formability behavior of steel used in ships by various methods", *Struct. Eng. Mech.*, **92**(2), 189-196.

https://doi.org/10.12989/sem.2024.92.2.189.
Sekban, D.M., Yaylacı, E.U., Özdemir, M.E., Öztürk, Ş., Yaylacı, M. and Panda, S.K. (2024), "Formability behavior of AH-32 shipbuilding steel strengthened by friction stir process", *Theor. Appl. Fract. Mech.*, **132**, 104485. https://doi.org/10.1016/j.tafmec.2024.104485.
Sekban, D.M., Yaylacı, E.U., Özdemir, M.E., Yaylacı, M. and Tounsi, A. (2025), "Investigating formability behavior of friction stir-welded high-strength shipbuilding steel using experimental, finite element, and artificial neural network methods", *J. Mater. Eng. Perform.*, **34**(6), 4942-4950. https://doi.org/10.1007/s11665-024-09501-8.
Selvamani, R., Ebrahimi, F., Yaylacı, M., Öztürk, Ş. and Yaylacı, E.U. (2024), "Nonlinear poro-thermo-forced vibration in curved sandwich magneto-electro-elastic shells under hygrothermal environment", *Acta Mechanica*, **235**(9), 5489-5528. https://doi.org/10.1007/s00707-024-03994-z.
Selvamani, R., Thangamuni, P., Yaylacı, M., Emin Özdemir, M. and Yaylacı, E.U. (2024), "Nonlinear vibration and parametric excitation of magneto-thermo elastic embedded nanobeam using homotopy perturbation technique", *ZAMM-J. Appl. Math. Mech./Zeitschrift für Angewandte Mathematik und Mechanik*, **104**(12), e202400525. https://doi.org/10.1002/zamm.202400525.
Singh, S. and Harsha, S.P. (2021), "Analysis of porosity effect on free vibration and buckling responses for sandwich sigmoid function based functionally graded material plate resting on Pasternak foundation using Galerkin Vlasov's method", *J. Sandw. Struct. Mater.*, **23**(5), 1717-1760. https://doi.org/10.1177/1099636220904340.
Sinha, G.P. and Kumar, B. (2021), "Review on vibration analysis of functionally graded material structural components with cracks", *J. Vib. Eng. Technol.*, **9**, 23-49. https://doi.org/10.1007/s42417-020-00208-3.
Slimani, R., Menasria, A., Ali Rachedi, M., Mourad, C., Refrafi, S., Nimer, A.A., Bouhadra, A. and Mamen, B. (2024), "A novel quasi-3D refined HSDT for static bending analysis of porous functionally graded Plates", *J. Comput. Appl. Mech.*, **55**(3), 519-537. https://doi.org/10.22059/jcamech.2024.372417.968.
Sun, G., Wang, Z., Yu, H., Gong, Z. and Li, Q. (2019), "Experimental and numerical investigation into the crashworthiness of metal-foam-composite hybrid structures", *Compos. Struct.*, **209**, 535-547. https://doi.org/10.1016/j.compstruct.2018.10.051.
Tamrabet, A., Mamen, B., Menasria, A., Bouhadra, A., Tounsi, A., Ghazwani, M.H., Alnujaie, A. and Mahmoud, S. (2023), "Buckling behaviors of FG porous sandwich plates with metallic foam cores resting on elastic foundation", *Struct. Eng. Mech.*, **85**(3), 289-304. https://doi.org/10.12989/sem.2023.85.3.289.
Tamrabet, A., Mourad, C., Ali Alselami, N., Menasria, A., Mamen, B. and Bouhadra, A. (2024), "Efficient kinematic model for stability analysis of imperfect functionally graded sandwich plates with ceramic middle layer and varied boundary edges", *J. Comput. Appl. Mech.*, **55**(2), 184-200. https://doi.org/10.22059/jcamech.2024.371464.947.
Tounsi, A., Bouhadra, A., Bousahla, A.A. and Mahmoud, S. (2017), "A new and simple HSDT for thermal stability analysis of FG sandwich plates", *Steel Compos. Struct.*, **25**(2), 157-175. https://doi.org/10.12989/scs.2017.25.2.157.
Tounsi, A., Bousahla, A.A., Tahir, S.I., Mostefa, A.H., Bourada, F., Al-Osta, M.A. and Tounsi, A. (2024), "Influences of different boundary conditions and hygro-thermal environment on the free vibration responses of FGM sandwich plates resting on viscoelastic foundation", *Int. J. Struct. Stab. Dyn.*, **24**(11), 2450117. https://doi.org/10.1142/S0219455424501177.
Tounsi, A., Kaci, A., Tounsi, A., Al-Osta, M.A., Yaylacı, M., Mohamed, S.M., Althobaiti, S. and Selim, M.M. (2025), "Quasi-3D plate theory for size-dependent static and free vibration analysis of FG microplate with porosities based on a modified couple stress theory", *Mech. Adv. Mater. Struct.*, 1-24. https://doi.org/10.1080/15376494.2025.2463687.
Tounsi, A., Mostefa, A.H., Attia, A., Bousahla, A.A., Bourada, F., Tounsi, A. and Al-Osta, M.A. (2023), "Free vibration investigation of functionally graded plates with temperaturedependent properties resting on a viscoelastic foundation", *Struct. Eng. Mech.*, **86**(1), 1-16. https://doi.org/10.12989/sem.2023.86.1.001.
Tounsi, A., Tahir, S.I., Al-Osta, M.A., Do-Van, T., Bourada, F., Bousahla, A.A. and Tounsi, A. (2023), "An integral quasi-3D computational model for the hygro-thermal wave propagation of imperfect FGM

sandwich plates", *Comput. Concrete*, **32**(1), 61-74. https://doi.org/10.12989/cac.2023.32.1.061.
Van Vinh, P. (2022), "Finite element analysis of functionally graded sandwich plates with porosity via a new hyperbolic shear deformation theory", *Def. Technol.*, **18**(3), 490-508. https://doi.org/10.1016/j.dt.2021.03.006.
Wang, Y.Q. and Zhang, Z.Y. (2019), "Bending and buckling of three-dimensional graphene foam plates", *Result. Phys.*, **13**, 102136. https://doi.org/10.1016/j.rinp.2019.02.072.
Wei, T., Lu, J., Zhang, P., Yang, G., Sun, C., Zhou, Y., Zhuang, Q. and Tang, Y. (2023), "Metal–organic framework-derived Co3O4 modified nickel foam-based dendrite-free anode for robust lithium metal batteries", *Chin. Chem. Lett.*, **34**(8), 107947. https://doi.org/10.1016/j.cclet.2022.107947.
Xiong, S., Zhou, C., Zhao, L., Zheng, X., Zhao, Y., Wang, B. and Li, R. (2022), "Symplectic framework-based new analytic solutions for thermal buckling of temperature-dependent moderately thick functionally graded rectangular plates", *Int. J. Struct. Stab. Dyn.*, **22**(14), 2250154. https://doi.org/10.1142/S0219455422501541.
Xiong, S., Zhou, C., Zheng, X., An, D., Xu, D., Hu, Z., Zhao, Y., Li, R. and Wang, B. (2022), "New analytic thermal buckling solutions of non-Lévy-type functionally graded rectangular plates by the symplectic superposition method", *Acta Mechanica*, **233**(7), 2955-2968. https://doi.org/10.1007/s00707-022-03258-8.
Yaylacı, M., Öner, E., Adıyaman, G., Öztürk, Ş., Uzun Yaylacı, E. and Birinci, A. (2024), "Analyzing of continuous and discontinuous contact problems of a functionally graded layer: Theory of elasticity and finite element method", *Mech. Bas. Des. Struct. Mach.*, **52**(8), 5720-5738. https://doi.org/10.1080/15397734.2023.2262562.
Yaylaci, M., Yaylaci, E.U., Turan, M., Ozdemir, M.E., Ozturk, S. and Ay, S. (2024), "Research of the crack problem of a functionally graded layer", *Steel Compos. Struct.*, **50**(1), 77-87. https://doi.org/10.12989/scs.2024.50.1.077.
Yaylacı, M., Yaylı, M., Öztürk, Ş., Ay, S., Özdemir, M.E., Yaylacı, E.U. and Birinci, A. (2024), "Examining the contact problem of a functionally graded layer supported by an elastic half-plane with the analytical and numerical methods", *Math. Meth. Appl. Sci.*, **47**(12), 10400-10420. https://doi.org/10.1002/MMA.10129.
Yaylacı, M., Yazıcıoğlu, A., Yaylacı, E.U., Terzi, M. and Birinci, A. (2025), "Evaluation of the contact problem of two layers one of functionally graded, loaded by circular rigid block and resting on a Pasternak foundation by analytical and numerical (FEM and MLP) methods", *Arch. Appl. Mech.*, **95**(4), **95**(4), 1-23. https://doi.org/10.1007/s00419-025-02787-7.
Yıldız, T. (2024), "Thermomechanical vibration response of solid and foam FGM nano actuator/sensor plates", *J. Vib. Eng. Technol.*, **12**, 1281-1297. https://doi.org/10.1007/s42417-024-01475-0.
Youzera, H., Meftah, S.A., Tounsi, A., Salem, M.A., Khedher, K.M. and Yaylacı, M. (2025), "Free vibration analysis of sandwich cylindrical shells with functionally graded carbon nanotube-reinforced composite face sheets using the differential quadrature (DQ) method", *Acta Mechanica*, **236**(2), 1395-1410. https://doi.org/10.1007/s00707-025-04230-y.
Zahari, K., Hilali, Y., Mesmoudi, S. and Bourihane, O. (2022). Review and comparison of thin and thick FGM plate theories using a unified buckling formulation. Structures,
Zenkour, A. and Radwan, A. (2020), "Bending and buckling analysis of FGM plates resting on elastic foundations in hygrothermal environment", *Arch. Civil Mech. Eng.*, **20**(4), 112. https://doi.org/10.1007/s43452-020-00116-z.
Zhou, J., Chang, X. and Li, Y. (2022), "Nonlinear vibration analysis of functionally graded flow pipelines under generalized boundary conditions based on homotopy analysis", *Acta Mechanica*, **233**(12), 5447-5463. https://doi.org/10.1007/s00707-022-03391-4.